symmetry

IMPACT FACTOR 2.7

CITESCORE 4.9

Article

The Single-Photon Scattering Properties of Three-Level Giant Atoms under the Interaction of Dissipation and Local Coupling

Liangwei Lin, Weiwei Zhang, Qipeng Cai, Yiguang Xu, Haipeng Yu, Xiaosheng Wang, Xiaohong Fang, Zixuan Chen, Yicai Zhang, Shengcan Ma et al.

MDPI

https://doi.org/10.3390/sym16020217

symmetry

MDPI

Article

The Single-Photon Scattering Properties of Three-Level Giant Atoms under the Interaction of Dissipation and Local Coupling

Liangwei Lin [1], Weiwei Zhang [1], Qipeng Cai [1], Yiguang Xu [1], Haipeng Yu [1], Xiaosheng Wang [1], Xiaohong Fang [1], Zixuan Chen [1], Yicai Zhang [2], Shengcan Ma [3] and Chaofei Liu [1,*]

[1] School of Science, Jiangxi University of Science and Technology, Ganzhou 341000, China; 6720210673@mail.jxust.edu.cn (L.L.); 6720210670@mail.jxust.edu.cn (W.Z.); 6120210297@mail.jxust.edu.cn (Q.C.); 6120231215@mail.jxust.edu.cn (Y.X.); 6120231231@mail.jxust.edu.cn (H.Y.); 6120231216@mail.jxust.edu.cn (X.W.); 6120231227@mail.jxust.edu.cn (X.F.); 6120231217@mail.jxust.edu.cn (Z.C.)
[2] School of Physics and Electronic Engineering, Guangzhou University, Guangzhou 510006, China; speezhangyicai@gzhu.edu.cn
[3] Faculty of Materials Metallurgy and Chemistry, Jiangxi University of Science and Technology, Ganzhou 341000, China; mashengcan@jxust.edu.cn
* Correspondence: liuchaofei@jxust.edu.cn

Abstract: The coupling of three-level giant atoms with one-dimensional waveguides can show interesting phenomena of transmission and reflection. Since the non-waveguide mode can cause the dissipation of external atoms, we consider the effect of the dissipation rate on the scattering of single photons in the system with giant atom–waveguide coupling. We find that as the dissipation rate of giant atoms increases, the transmission rate of a single photon increases and the reflection rate decreases. In addition, by varying the phase difference and decay rate, the giant atoms are able to achieve perfect transmission and total reflection over the entire frequency range. We also find and show the conditions for the conversion of the optimal frequency. When the cumulative phase of photons reaches a certain value, the system can achieve perfect transmission, which is independent of frequency. This model of coupling giant atoms with waveguides has a promising application in quantum communication and quantum information processing.

Keywords: giant atom; scattering properties; dissipation rate; one-dimensional waveguide; the total reflection

Citation: Lin, L.; Zhang, W.; Cai, Q.; Xu, Y.; Yu, H.; Wang, X.; Fang, X.; Chen, Z.; Zhang, Y.; Ma, S.; et al. The Single-Photon Scattering Properties of Three-Level Giant Atoms under the Interaction of Dissipation and Local Coupling. *Symmetry* **2024**, *16*, 217. https://doi.org/10.3390/sym16020217

Academic Editor: Fabio Cardone

Received: 27 November 2023
Revised: 25 January 2024
Accepted: 31 January 2024
Published: 11 February 2024

1. Introduction

A giant atom is an artificial atom that is essentially a superconducting circuit. Similar to natural atoms, the giant atom can obtain electrons, get excited, and then give off their energy by emitting light. And the main novelty of the giant atom is that the interference effects generated by multiple coupling points are not present in the quantum optics of ordinary small atoms. Since the size of the radius of the natural atom is negligible compared to the wavelength of the waveguide mode, in general, the natural atom can be regarded as a point when coupled to the waveguide. However, when superconducting transmission qubits are designed to interact with surface acoustic waves (SAWs) through multiple coupling points, the separation distances of these coupling points can be much greater than the wavelength of SAWs [1]. So, the "giant atom" theory was mainly developed to describe this case [2]. Since the first theoretical study in 2014 [3], the giant atom scheme has been extensively studied by superconducting qubits [4–8], coupled waveguide arrays [9], and cold atoms [10]. Through the non-local coupling scheme, a series of tantalizing quantum phenomena have been demonstrated, including frequency-dependent relaxation rates and Lamb shifts [3,7,11], non-exponential atomic decay [4,5], decoherence-free interatomic interactions [7,12,13], singular bound states [6,14], and modified topological effects [15].

Giant atoms have emerged as a new paradigm for quantum optics that could promote a more complete understanding of physics.

Waveguide quantum electrodynamics (QED) studies the interactions between atoms and one-dimensional waveguide modes, and it is an important system for studying the interaction between light and matter. Waveguide QED system can not only be used to construct remote interaction and engineer large-scale quantum networks [16–20] but can also be a good platform for manipulating single-photon transmission [21–26]. Typical methods for implementing waveguide QED systems include quantum dots coupled to photonic crystal waveguides [27,28], superconducting qubits coupled to transmission lines [29,30], and ultracold atoms coupled to optical fibers [31,32]. Traditional waveguide QED mainly studies the interaction between small atoms and waveguides. However, with the emergence of giant atoms, it has been found that giant atoms can have multiple nodes coupled with waveguides, resulting in a series of interesting phenomena different from small atoms, such as multiple reflections and transmission of photons among multiple coupling points.

In previous works, Chen et al. [33] have reported the coupling of two-level giant atoms to one-dimensional waveguides, Du et al. [34] have studied the coupling of three-level giant atoms and one-dimensional waveguides, and ref. [12] has shown that when two woven giant atoms are coupled with a waveguide, there is decoherence-free interatomic interaction. In addition, Cai et al. [11] studied the coupling of a giant atom to a one-dimensional waveguide at multiple points. In this work, the scattering properties of a single photon, including the total reflection and perfect transmission, are studied by coupling a giant Λ-type atom with a waveguide. On the basis of the coupling model of a single giant atom and a one-dimensional waveguide, we add the dissipative and local coupling phases to study the scattering characteristics of a single photon and study the frequency conversion of single photons under the interference of three-level giant atoms.

The structure of this paper is as follows. In Section 2, we introduce the model and the Hamiltonian and give a strict calculation process. In Section 3, we analyze the model in detail and give a large number of results on the transmission and reflection of single photons. In Section 4, we summarize this work and analyze the application prospect of this work.

2. Model and the Hamiltonian

As shown in Figure 1, we consider a large Λ-type three-level atom coupled with a single one-dimensional waveguide at two points. $|g\rangle \leftrightarrow |e\rangle$ and $|f\rangle \leftrightarrow |e\rangle$ are the two kinds of transformation of the atoms, and the waveguide is coupled through two coupling points located at $x_1 = -d/2$ and $x_2 = d/2$, where $|g\rangle$, $|f\rangle$, and $|e\rangle$ are ground state, intermediate state, and excited state, respectively. The atom–waveguide coupling coefficients are $g_1 e^{i\theta_1}$ and $g_2 e^{i\theta_2}$, respectively. The locally coupled phases θ_1 and θ_2 and the coupling intensities g_1 and g_2 can produce some interesting interference effects on the scattering properties, which will be discussed below. We can use superconducting quantum devices, and the locally coupled phase can be introduced through Josephson rings of external flux threads [35].

Under rotating wave approximation (RWA), the real-space Hamiltonian of the model can be written as ($\hbar = 1$)

$$H = H_\omega + H_a + H_I,$$

$$H_\omega = \int_{-\infty}^{+\infty} dx \left[a_L^\dagger(x) \left(\omega_0 + i v_g \frac{\partial}{\partial x} \right) a_L(x) + a_R^\dagger(x) \left(\omega_0 - i v_g \frac{\partial}{\partial x} \right) a_R(x) \right],$$

$$H_a = \omega_f |f\rangle\langle f| + (\omega_e - i\gamma) |e\rangle\langle e|,$$

$$H_I = \int_{-\infty}^{+\infty} dx P(x) \left\{ g_1 e^{i\theta_1} \left[a_R^\dagger(x) + a_L^\dagger(x) \right] |g\rangle\langle e| + g_2 e^{i\theta_2} \left[a_R^\dagger(x) + a_L^\dagger(x) \right] |f\rangle\langle e| + H.c. \right\}, \quad (1)$$

where $P(x) = \delta(x + d/2) + \delta(x - d/2)$, H_ω represents the free Hamiltonian of the waveguide mode, and v_g is the group velocity of the photons in the waveguide. In addition, $a_{R,L}$ ($a^+_{R,L}$) are the boson annihilation (production) operators of the right and left photons in the waveguide, respectively. ω_0 is the frequency of the waveguide [1,36]. H_a is the Hamiltonian of the atom, where ω_f is the frequency between the ground state $|g\rangle$ and intermediate state $|f\rangle$ transition, ω_e is the frequency between the ground state $|g\rangle$ and excited state $|e\rangle$ transition. γ is the rate of external atomic dissipation due to non-waveguide modes in the environment. H_I describes the interaction between atoms and waveguides, where the Dirac functions $\delta(x + d/2)$ and $\delta(x - d/2)$ indicate that the atom–waveguide coupling occurs at $x = -d/2$ and $x = d/2$, respectively. In addition, there is an accumulated photon phase between two coupling points $\phi_1 = kd$ and $\phi_2 = qd$, where k and q are renormalized wave vectors that satisfy the linearized dispersion relationship, and $E = \omega_0 + kv_g$.

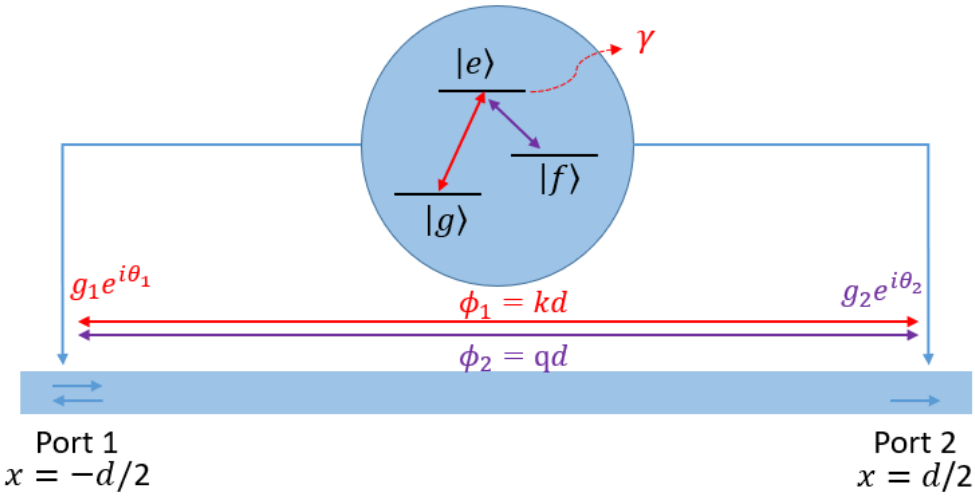

Figure 1. Structure diagram of a three-level giant atom coupled at $x = -d/2$ and $x = d/2$, with separate local coupling phases θ_1 and θ_2 and coupling intensities g_1 and g_2. The blue one-way arrows indicate that the photons may be transmitted or reflected when it is incident from the left.

Due to the conservation of the total excitation number in RWA, the eigenstates of the system can be represented as

$$|\psi\rangle = \sum_{\alpha=g,f} \int_{-\infty}^{+\infty} dx \Big[R_\alpha(x) a_R^\dagger(x) |0,\alpha\rangle + L_\alpha(x) a_L^\dagger(x) |0,\alpha\rangle \Big] + u_e |0,e\rangle, \tag{2}$$

where $R_\alpha(x)$ [$L_\alpha(x)$] is in the position of x waveguide to create the probability amplitude of the right-moving (left-moving) photons, and the atoms are in the state $|\alpha\rangle$ eventually. In addition, u_e is the probability amplitude of excited atoms. By solving the Schr?dinger equation $H|\psi\rangle = E|\psi\rangle$, we can obtain the following probability amplitude equation:

$$\begin{aligned}
ER_g(x) &= \left(\omega_0 - iv_g \frac{\partial}{\partial x}\right) R_g(x) + g_1 e^{i\theta_1} P(x) u_e \\
EL_g(x) &= \left(\omega_0 - iv_g \frac{\partial}{\partial x}\right) L_g(x) + g_1 e^{i\theta_1} P(x) u_e \\
ER_f(x) &= \left(\omega_f - iv_g \frac{\partial}{\partial x}\right) R_f(x) + g_2 e^{i\theta_2} P(x) u_e \\
EL_f(x) &= \left(\omega_f - iv_g \frac{\partial}{\partial x}\right) L_f(x) + g_2 e^{i\theta_2} P(x) u_e \\
Eu_e &= (\omega_e - i\gamma) u_e + g_1 e^{-i\theta_1} P(x) \big[R_g(x) + L_g(x) \big] + g_2 e^{-i\theta_2} \Big[R_f(x) + L_f(x) \Big],
\end{aligned} \tag{3}$$

We first assume that the wave vector $k(k > 0)$ of a single photon from the left of the waveguide, and the atom is initialized in the ground state $|g\rangle$. The wave function can be written as

$$\begin{aligned}
R_g(x) &= e^{ikx}\left\{\Theta\left(-x-\frac{d}{2}\right)+A\left[\Theta\left(x+\frac{d}{2}\right)-\Theta\left(x-\frac{d}{2}\right)\right]+t_1\Theta\left(x-\frac{d}{2}\right)\right\},\\
L_g(x) &= e^{-ikx}\left\{r_1\Theta\left(-x-\frac{d}{2}\right)+B\left[\Theta\left(x+\frac{d}{2}\right)-\Theta\left(x-\frac{d}{2}\right)\right]\right\},\\
R_f(x) &= e^{iqx}\left\{M\left[\Theta\left(x+\frac{d}{2}\right)-\Theta\left(x-\frac{d}{2}\right)\right]+t_2\Theta\left(x-\frac{d}{2}\right)\right\},\\
L_f(x) &= e^{-iqx}\left\{r_2\Theta\left(x-\frac{d}{2}\right)+N\left[\Theta\left(x+\frac{d}{2}\right)-\Theta\left(x-\frac{d}{2}\right)\right]\right\},
\end{aligned} \tag{4}$$

where $q = k - \omega_f/v_g$, and $\Theta(x)$ is the Heaviside step function. In addition, A and B (M and N) are the probability amplitudes of a right-moving photon and a left-moving photon in the $x_1 < x < x_2$ region, respectively. Finally, the atoms are in the state $|g\rangle$ ($|f\rangle$). For cases where the frequency is fixed (i.e., the final state of the atom is $|g\rangle$), we define t_1 and r_1 as the transmission and reflection amplitudes of the input photons, respectively. For frequency conversion conditions (i.e., the final state of the atom is $|f\rangle$), we define t_2 and r_2 as the conversion amplitudes of the output photons of the wave vectors q and $-q$, respectively.

We substitute Equation (4) into Equation (3) and obtain the following equations:

$$\begin{aligned}
0 &= -iv_g(A-1)e^{-ikd/2}+g_1e^{i\theta_1}u_e\\
0 &= -iv_g(t_1-A)e^{ikd/2}+g_1e^{i\theta_1}u_e\\
0 &= -iv_g(r_1-B)e^{ikd/2}+g_1e^{i\theta_1}u_e\\
0 &= -iv_gBe^{-ikd/2}+g_1e^{i\theta_1}u_e\\
0 &= -iv_gMe^{-iqd/2}+g_2e^{i\theta_2}u_e\\
0 &= -iv_g(t_2-M)e^{iqd/2}+g_2e^{i\theta_2}u_e\\
0 &= -iv_g(r_2-N)e^{iqd/2}+g_2e^{i\theta_2}u_e\\
0 &= -iv_gNe^{-iqd/2}+g_2e^{i\theta_2}u_e\\
0 &= \tfrac{g_1}{2}e^{-i\theta_1}\left[(A+B+1)e^{-ikd/2}+(A+B+t_1+r_1)e^{ikd/2}\right]+\\
&\quad \tfrac{g_2}{2}e^{-i\theta_2}\left[(M+N)e^{-iqd/2}+(M+N+t_2+r_2)e^{iqd/2}\right]-(\Delta+i\gamma)u_e,
\end{aligned} \tag{5}$$

Next, we simplify the equations above and obtain

$$A = 1+\frac{g_1e^{i\theta_1}u_e}{iv_ge^{-i\phi_1/2}}$$

$$t_1 = 1+\frac{g_1e^{i\theta_1}u_e}{iv_ge^{i\phi_1/2}}+\frac{g_1e^{i\theta_1}u_e}{iv_ge^{-i\phi_1/2}}$$

$$r_1 = \frac{g_1e^{i\theta_1}u_e}{iv_ge^{i\phi_1/2}}+\frac{g_1e^{i\theta_1}u_e}{iv_ge^{-i\phi_1/2}}$$

$$B = \frac{g_1e^{i\theta_1}u_e}{iv_ge^{-i\phi_1/2}}$$

$$M = \frac{g_2 e^{i\theta_2} u_e}{i v_g e^{-i\phi_2/2}}$$

$$t_2 = \frac{g_2 e^{i\theta_2} u_e}{i v_g e^{i\phi_2/2}} + \frac{g_2 e^{i\theta_2} u_e}{i v_g e^{-i\phi_2/2}}$$

$$r_2 = \frac{g_2 e^{i\theta_2} u_e}{i v_g e^{i\phi_2/2}} + \frac{g_2 e^{i\theta_2} u_e}{i v_g e^{-i\phi_2/2}}$$

$$N = \frac{g_2 e^{i\theta_2} u_e}{i v_g e^{-i\phi_2/2}}$$

$$u_e = \frac{2 g_1 e^{-i\theta_1} cos(\phi_1/2)}{\Delta + i\gamma + 2i\Gamma_1\left(1 + e^{i\phi_1}\right) + 2i\Gamma_2\left(1 + e^{i\phi_2}\right)}, \tag{6}$$

where $\Delta = E - \omega_e$ is the frequency detuning between the incident photon and the frequency of the atomic transition ($|g\rangle \leftrightarrow |e\rangle$). Then, by solving Equation (6), the transmission amplitude can be obtained as (see Appendix A for more details)

$$t_1 = \frac{\Delta + i\gamma - 2\Gamma_1 sin\phi_1 + 2i\Gamma_2\left(1 + e^{i\phi_2}\right)}{\Delta + i\gamma + 2i\Gamma_1\left(1 + e^{i\phi_1}\right) + 2i\Gamma_2\left(1 + e^{i\phi_2}\right)}, \tag{7}$$

where $\phi_1 = kd$ and $\phi_2 = qd$ are the accumulated phase of photons transmitted between the two coupled points by the wave vectors k and q, respectively. Here, $\Gamma_1 = g_1^2/v_g$ ($\Gamma_2 = g_2^2/v_g$) is the radiative decay rate from the excited state $|e\rangle$ to a lower-energy state $|g\rangle$ ($|f\rangle$) contributed from each atom–waveguide coupling point [34]. When $d = 0$, the transmission amplitude in Equation (6) can be simplified as

$$t_1 = \frac{\Delta + i\gamma - 2\Gamma_1 sin\phi_1}{\Delta + i\gamma + 4i\Gamma_1 + 4i\Gamma_2}. \tag{8}$$

It restores the energy of a small Λ-type atom [37]. Because there are two coupling points, the radiation decay rate here is quadrupled. In addition, the transmission amplitude becomes

$$t_1 = \frac{\Delta + i\gamma + 4i\Gamma_2}{\Delta + i\gamma + 2i\Gamma_1\left(1 + e^{i\phi_1}\right)}. \tag{9}$$

In the case of $\Gamma_2 = 0$ (i.e., $g_2 = 0$), this is exactly the same as a giant two-level atom [38]. Similarly, we can obtain the other scattering amplitudes

$$r_1 = \frac{-i\Gamma_1 (2cos(\phi_1/2))^2}{\Delta + i\gamma + 2i\Gamma_1\left(1 + e^{i\phi_1}\right) + 2i\Gamma_2\left(1 + e^{i\phi_2}\right)} \tag{10a}$$

$$t_2 = r_2 = \frac{-i\sqrt{\Gamma_1\Gamma_2}(2cos(\phi_1/2))(2cos(\phi_2/2))e^{-i\theta}}{\Delta + i\gamma + 2i\Gamma_1\left(1 + e^{i\phi_1}\right) + 2i\Gamma_2\left(1 + e^{i\phi_2}\right)}, \tag{10b}$$

where $\theta = \theta_1 - \theta_2$ is the phase difference between the two atomic waveguide coupling channels. Similarly, when $d = 0$ and $\Gamma_2 = 0$, the amplitude in Equations (10a,b) can be reduced to the amplitude of the small Λ atom and that of the large two-level atom, respectively. Obviously, photon number is conserved (i.e., $|t_1|^2 + |r_1|^2 + |t_2|^2 + |r_2|^2 = 1$), and the model has internal symmetry (i.e., $|t_2|^2 \equiv |r_2|^2$). Now, we define $T_1 = |t_1|^2$ and $R_1 = |r_1|^2$, where T_1 and R_1 are the transmission rate and reflection rate, respectively, and the conversion efficiency is $T_c = |t_2|^2 + |r_2|^2$.

3. Result Analysis

We first investigate the dependence of the scattering probabilities on ϕ_1 and $\Delta\phi = \phi_1 - \phi_2$, both of which can be adjusted experimentally. Figure 2 is a three-dimensional plot of the scattering probability with detuning Δ and phase difference $\Delta\phi$. In Figure 2,

we can see that the position and minimum (maximum) of T_1 (R_1 and T_c) with $\Delta\phi$ vary periodically with a period of 2π. We find that the transmission rate T_1 varies periodically with $\Delta\phi$, and the period is just 2π. Similarly, the reflection rate R_1 and the conversion efficiency T_c also have these properties.

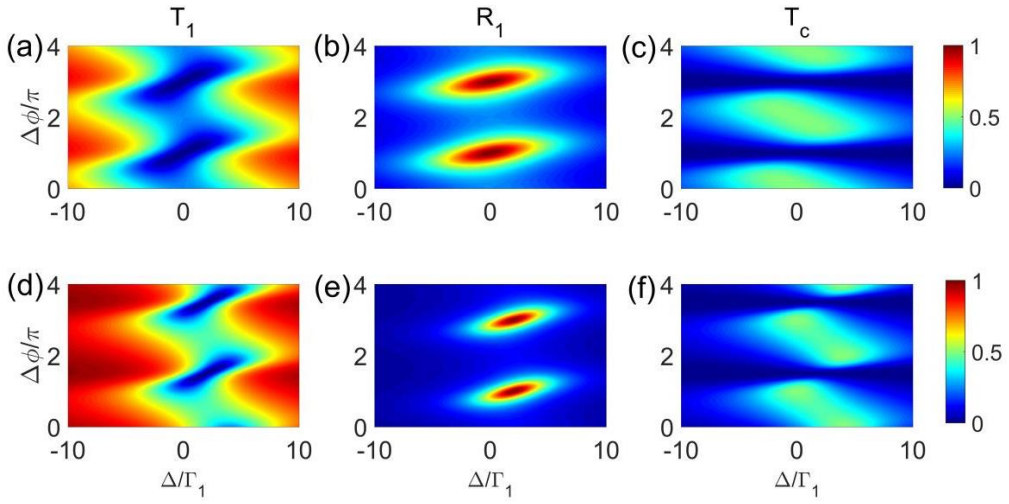

Figure 2. The effect of phase on the transmission rate T_1, reflection rate R_1, and conversion efficiency T_c with different detuning Δ/Γ_1 and phase difference $\Delta\phi$. (**a**,**d**) The transmission rate T_1, (**b**,**e**) the reflection rate R_1, (**c**,**f**) conversion efficiency T_c. We set the phase $\phi_1 = 0$ in (**a**–**c**) and $\phi_1 = \pi/2$ in (**d**–**f**). Other parameters are $\eta = 1$, $\gamma/\Gamma_1 = 0$, $\theta = 0$.

In Figure 2a, we find that the minimum value of T_1 occurs at $\Delta = 0$ (i.e., $T_1(\Delta = 0) = 0$) when $\phi_1 = 0$ and $\Delta\phi = \pi$ or 3π. In addition, for a fixed value $\Delta\phi$, as the value of $|\Delta/\Gamma_1|$ increases, the value of the transmission rate T_1 increases.

In Figure 2b, the maximum point of R_1 occurs at $\Delta = 0$ and $\Delta\phi = \pi$ or 3π, where $R_1(\Delta = 0) = 1$. Different from the transmission rate T_1, the reflection rate R_1 gradually decreases with an increase in $|\Delta/\Gamma_1|$ at a given value of $\Delta\phi$. In Figure 2c, we find that the conversion efficiency $T_c \equiv 0$, which is regardless of the change in the value of Δ/Γ_1 when $\phi_1 = 0$ and$\Delta\phi = \pi$ or 3π. Additionally, when $T_c(\Delta = 0) = 0.5$, this case also occurs at $\Delta\phi = 0$ or 2π. Comparing Figure 2a–c, we find that the total reflection is achieved at $\Delta = 0$ when $\phi_1 = 0$ and $\Delta\phi = \pi$ or 3π. Similarly, when the phase ϕ_1 increases to $\pi/2$ and $\Delta\phi = 3\pi/2$ or $5\pi/2$, as shown in Figure 2d–f, the total reflection point deviates, occurring at $\Delta = 2\Gamma_1$. In fact, we find that the reflection rate, transmission rate, and conversion efficiency all change with a period of 2π at different phases.

To more intuitively observe the transmission rate T_1, reflection rate R_1, and conversion efficiency T_c, we plot the variation trends of these values with detuning Δ and we choose the phase difference $\Delta\phi = 0, \pi/2, \pi, 3\pi/2$ (see Figure 3).

Figure 3a shows the transmission rate with detuning Δ at phase $\phi_1 = 0$. Obviously, the transmission rate curve is convex downward. The minimum value of the transmission rate occurs at $\Delta = 0$ and $\Delta\phi = \pi$, which is 0. Figure 3b,c show the values of the reflection rate and conversion efficiency curves with detuning Δ for phase $\phi_1 = 0$, respectively. In contrast, in Figure 3a–c, we find $T_1(\Delta = 0) = 0$, $R_1(\Delta = 0) = 1$, and $T_c(\Delta = 0) = 0$ when $\phi_1 = 2m\pi$ and $\Delta\phi = \pi$. These results show that total reflection occurs. In this case, the transition of $|g\rangle \leftrightarrow |e\rangle$ is completely suppressed due to the destructive interference of the two corresponding decay channels, i.e., $\Gamma_2[1 + exp(i\phi_2)] = 0$. Thus, the model can be reduced to the two-level atom coupled with the one-dimensional waveguide, where the resonant incident photon is fully reflected. For $\phi_1 = (2m + 1/2)\pi$, the total reflection condition is $\Delta\phi = 3\pi/2$, $\Delta = 2\Gamma_1$, as shown in Figure 3d–f.

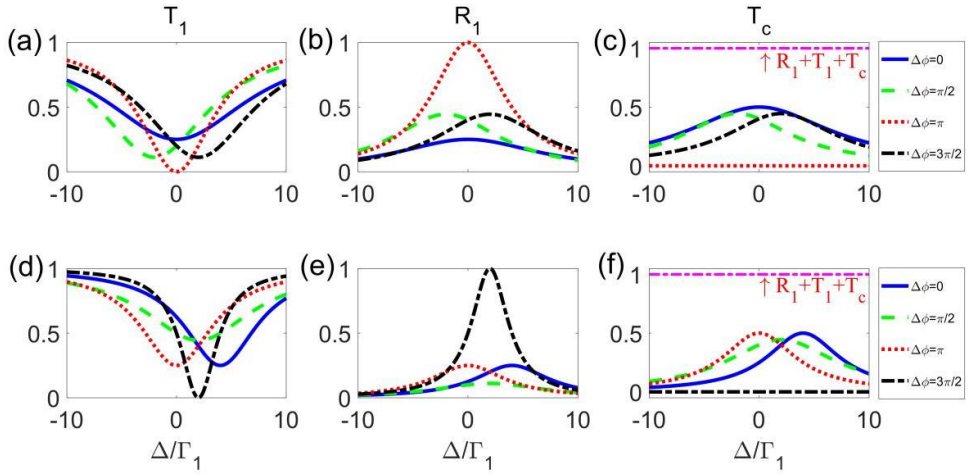

Figure 3. The changing process of transmission rate T_1, reflection rate R_1, and conversion efficiency T_c with different detuning Δ/Γ_1 at different phases. (**a**,**d**) The transmission rate T_1, (**b**,**e**) the reflection rate R_1, (**c**,**f**) the conversion efficiency T_c. We set the phase $\phi_1 = 0$ in (**a**–**c**) and $\phi_1 = \pi/2$ in (**d**–**f**). Other parameters are $\eta = 1$, $\gamma/\Gamma_1 = 0$, $\theta = 0$.

In fact, as long as $\phi_2 = \phi_1 - \Delta\phi = (2m+1)\pi$, we can observe the total reflection. More interestingly, when $\phi_1 = (2m+1)\pi$, no matter how the value of $\Delta\phi$ changes, the system achieves frequency-independent perfect transmission (FIPT), i.e., $T_1(\Delta) \equiv 1$ and $R_1(\Delta) = T_c(\Delta) \equiv 0$. In addition, based on the pink dotted curves in Figure 3c,f, we can see that no matter how the value of $\Delta\phi$ changes, $T_1 + R_1 + T_c \equiv 1$. This phenomenon actually comes from the conservation of the number of photons in the system.

We further change the phase difference [$\Delta\phi \in [0, 2\pi)$] and investigate the change in the transmission rate T_1, reflection rate R_1, and conversion efficiency T_c with the change in $\Delta\phi$ (see Figure 4).

In Figure 4a, we find that when $\phi_1 = 0$ and $\Delta\phi = \pi$, the minimum value of the transmission rate T_1 is 0, the maximum value of the reflection rate R_1 is 1, and the maximum value of the conversion efficiency T_c is 0. The results indicate that the system achieves total reflection. When the phase ϕ_1 increases to $\pi/2$ [see Figure 4b], the total reflection occurs at $\Delta\phi = 3\pi/2$. With ϕ_1 increasing to π [see Figure 4c], the minimum value of the transmission rate T_1 is 1, the maximum value of the reflection rate R_1 is 0, and the maximum value of the conversion efficiency T_c is 0. They do not change with $\Delta\phi$. And we find that when $\phi_1 = (2m+1)\pi$, the transmission rate of the system is always 1 and the reflection rate is always 0. This shows that the incident photon is completely transmitted and the system achieves perfect transmission, which is independent of frequency (FIPT). In Figure 4d, when $\phi_1 = 3\pi/2$ and $\Delta\phi = \pi/2$, the minimum value of the transmission rate T_1 is 0, the maximum value of the reflection rate R_1 is 1, and the maximum value of the conversion efficiency T_c is 0. Total reflection occurs at $\Delta\phi = 3\pi/2$.

Previous studies have shown that in the case of small atoms, the scattering probability is completely determined by the decay ratio $\eta = \Gamma_2/\Gamma_1$ [37,39]. However, in the case of giant atoms, the scattering probability is not only determined by the decay ratio $\eta = \Gamma_2/\Gamma_1$ but is also dependent on phase. Therefore, we will continue to plot the scattering probability with respect to the decay ratio $\eta = \Gamma_2/\Gamma_1$ and the phase difference $\Delta\phi = \phi_1 - \phi_2$ (see Figure 5).

Figure 5 depicts the scattering probability as a function of detuning Δ and decay rate η. In Figure 5a, we find that when $\Delta\phi = 0$ and $\eta = 0$, the minimum point of the transmission rate occurs at $\Delta = 0$ (i.e., $T_1(\Delta = 0) = 0$). In addition, when η is a fixed value, the transmission rate T_1 increases with an increase in $|\Delta/\Gamma_1|$. In Figure 5b, the maximum of the reflection rate occurs at $\Delta = 0$ and $\eta = 0$. At this time, the system has $R_1(\Delta = 0) = 1$. Different from the transmission rate T_1, the reflection rate R_1 decreases with an increase in $|\Delta/\Gamma_1|$ when η is fixed. In Figure 5c, we find that the best frequency transition ($T_c = 0.5$)

occurs at $\Delta = 0$ and $\eta = 1$. The phenomenon is the same as that of the small atoms. In addition, with an increase in $|\Delta/\Gamma_1|$, the conversion efficiency T_c decreases gradually.

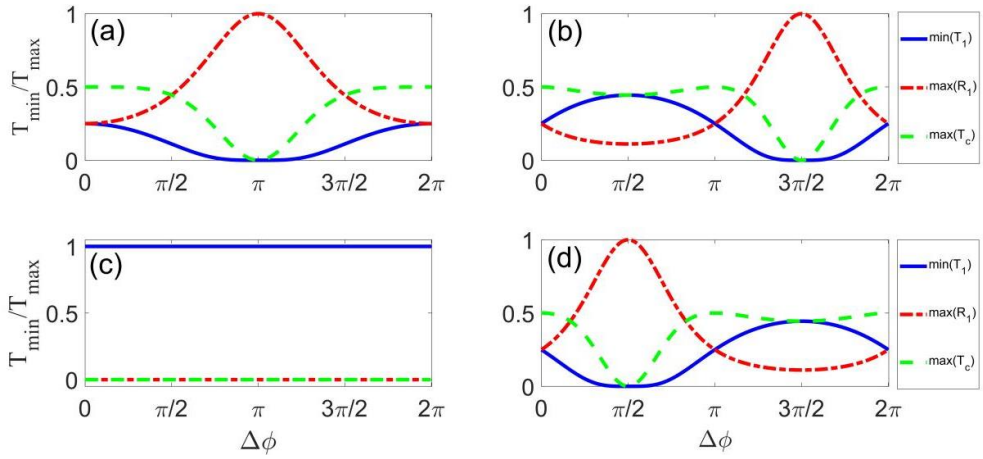

Figure 4. The effect of phase on the extreme values of transmission rate T_1, reflection rate R_1, and conversion efficiency T_c with different phase differences $\Delta\phi$. (**a**) The phase is set to be $\phi_1 = 0$, (**b**) $\phi_1 = \pi/2$, (**c**) $\phi_1 = \pi$, and (**d**) $\phi_1 = 3\pi/2$. Other parameters are $\eta = 1$, $\gamma/\Gamma_1 = 0$, $\theta = 0$.

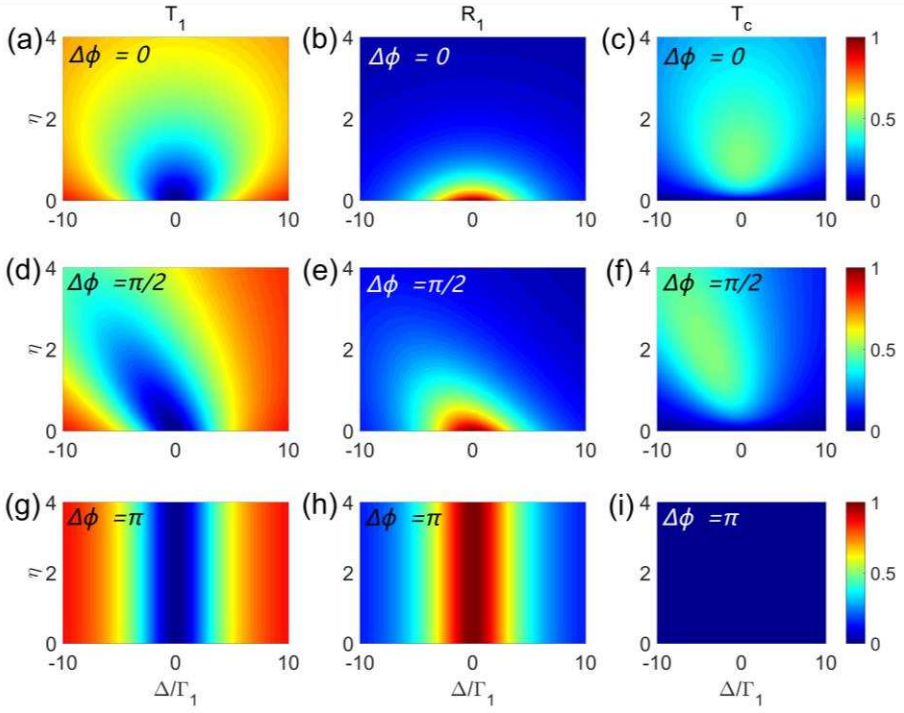

Figure 5. The effect of phase difference on the transmission rate T_1, reflection rate R_1, and conversion efficiency T_c with different detuning Δ/Γ_1 and decay rate η. (**a**,**d**,**g**) The transmission rate T_1, (**b**,**e**,**h**) the reflection rate R_1, (**c**,**f**,**i**) the conversion efficiency T_c. We set the phase difference $\Delta\phi = 0$ in (**a**–**c**), $\Delta\phi = \pi/2$ in (**d**–**f**), and $\Delta\phi = \pi$ in (**g**–**i**). Other parameters are $\phi_1 = 0$, $\gamma/\Gamma_1 = 0$, $\theta = 0$.

When the phase difference $\Delta\phi$ increases to $\pi/2$, the minimum of the transmission rate occurs at $\Delta = 0$ and $\eta = 0$ [see Figure 5d], and the value is 0. In addition, the transmission rate T_1 increases with an increase in $|\Delta/\Gamma_1|$. In Figure 5e, we find that the maximum of the reflection rate (i.e., $R_1 = 1$) also occurs at $\Delta = 0$ and $\eta = 0$. As in the case of $\Delta\phi = 0$, the minimum value of the transmission rate and maximum value of the reflection rate of the system occur at $\Delta = 0$ and $\eta = 0$. The difference is that the optimal frequency conversion

of the system has deviated. The best transition of the frequency occurs at $\Delta = -4\Gamma_1$ and $\eta = 2$ [see Figure 5f].

When $\Delta\phi = \pi$ [see Figure 5g–i], we find that the transmission rate T_1, reflection rate R_1, and conversion efficiency T_c are independent of η. This phenomenon indicates that the frequency conversion is completely suppressed.

In order to more intuitively observe the variation trends of the transmission rate T_1, reflection rate R_1, and conversion efficiency T_c with respect to detuning Δ and decay rate η, we set η to 0, 1, 2, and 3, respectively, and draw Figure 6.

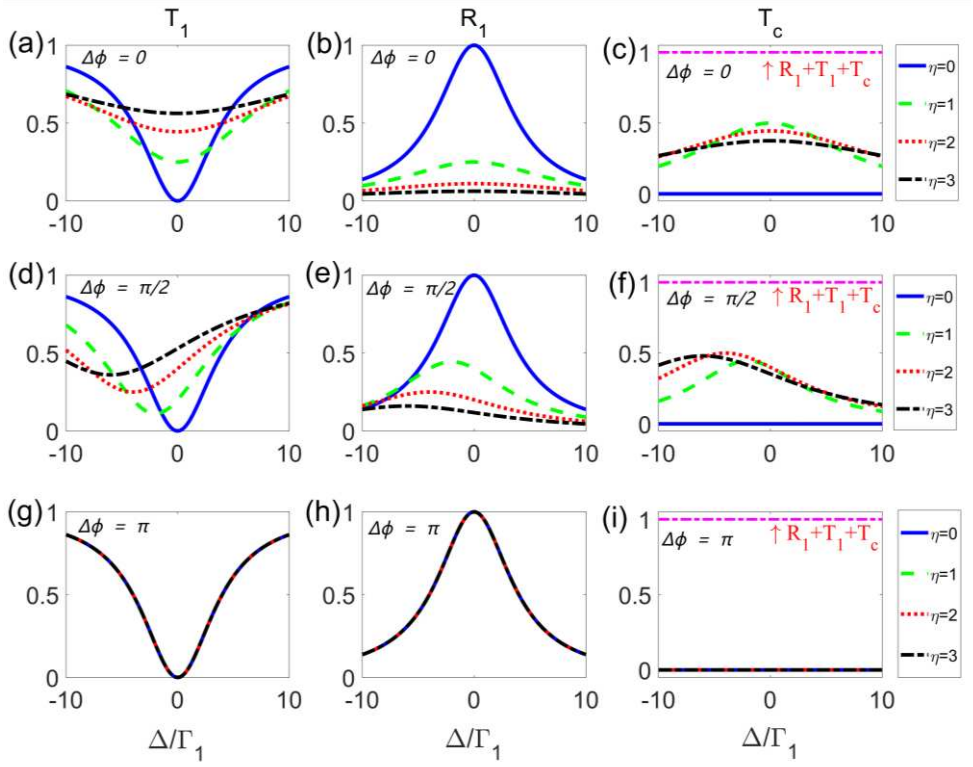

Figure 6. The changing process of transmission rate T_1, reflection rate R_1, and conversion efficiency T_c with different detuning Δ/Γ_1 at different phase differences. (**a**,**d**,**g**) The transmission rate T_1, (**b**,**e**,**h**) the reflection rate R_1, (**c**,**f**,**i**) the conversion efficiency T_c. We set the phase difference $\Delta\phi = 0$ in (**a**–**c**), $\Delta\phi = \pi/2$ in (**d**–**f**), and $\Delta\phi = \pi$ in (**g**–**i**). Other parameters are $\phi_1 = 0$, $\gamma/\Gamma_1 = 0$, $\theta = 0$.

Figure 6 shows the curves of scattering rate with detuning Δ at different phase differences $\Delta\phi$. In Figure 6a, the minimum value of the transmission rate occurs at $\Delta = 0$ and $\eta = 0$, which is 0. Figure 6b,c show the variation trend of the reflection rate and conversion efficiency with detuning Δ at phase difference $\Delta\phi = 0$, respectively. In Figure 6c, we find that the optimal transition frequency of the system occurs at $\Delta = 0$ and $\eta = 1$ (dashed green lines). In contrast, in Figure 6a–c, when the $\Delta\phi = 0$ and $\eta = 0$, we found that $T_1(\Delta = 0) = 0$, $R_1(\Delta = 0) = 1$, $T_c(\Delta = 0) = 0$. The results show that total reflection occurs.

Figure 6d–f show the curves of scattering rate with detuning Δ at different phase differences $\Delta\phi$. When $\Delta\phi = \pi/2$, the minimum system transmission rate ($T_1 = 0$) appears at $\Delta = 0$ and $\eta = 0$ [see solid blue line in Figure 6d]. In Figure 6e, we find that the maximum value of the system reflection rate ($R_1 = 1$) also occurs at $\Delta = 0$ and $\eta = 0$. This phenomenon shows that the total reflection of the system occurs under the conditions $\Delta = 0$ and $\eta = 0$ when $\Delta\phi = \pi/2$. However, unlike those in the case of $\Delta\phi = 0$, the optimal frequency conversion of the system occurs at $\Delta = -4\Gamma_1$ and $\eta = 2$ [see red dashed line in Figure 6f]. In addition, based on the pink dotted curves in Figure 6c,f,i, we can see that no matter how the value of $\Delta\phi$ changes, $T_1 + R_1 + T_c \equiv 1$.

In fact, the best frequency conversion ($T_c = 0.5$) occurs at $\Delta = 0$ and $\eta = 1$ when $\phi_1 = 2m\pi$ and $\Delta\phi = 0$ [see Figure 6a–c]. It is the same as the behaviors of small atoms. With an increase in $|\Delta/\Gamma_1|$, the conversion efficiency T_c decreases gradually. When $\phi_1 = 2m\pi$ and $\Delta\phi = \pi$ [see Figure 6g–i], the frequency conversion is completely suppressed. The incoming photons of the system are completely reflected. In this case, all scattering probabilities are independent of η. When $\phi_1 = 2m\pi$ and $\Delta\phi = \pi/2$ (see Figure 6d–f), the best frequency conversion ($T_c = 0.5$) appears in the $\Delta = -4\Gamma_1$ and $\eta = 2$.

We further change the decay ratio and study the changes of transmission rate T_1, reflection rate R_1, and conversion efficiency T_c with η values changing [see Figure 7]. In Figure 7a, we find that the minimum of the transmission rate T_1 is monotonically increasing when $\phi_1 = 0$ and $\Delta\phi = 0$. Its minimum value occurs at $\eta = 0$, which is 0. The maximum value of the reflection rate R_1 and the maximum value of the conversion efficiency T_c are monotone decreasing curves. Both of the maximums occur at $\eta = 0$ and the values are 1. However, when the phase difference $\Delta\phi$ increases to $\pi/2$ [see Figure 7b], the minimum of the transmission rate T_1 has a constant value of 0 no matter how the value of η changes. The maximum value of the reflection rate R_1 is a monotone decline curve, and its maximum value occurs at $\eta = 0$, which is 1.

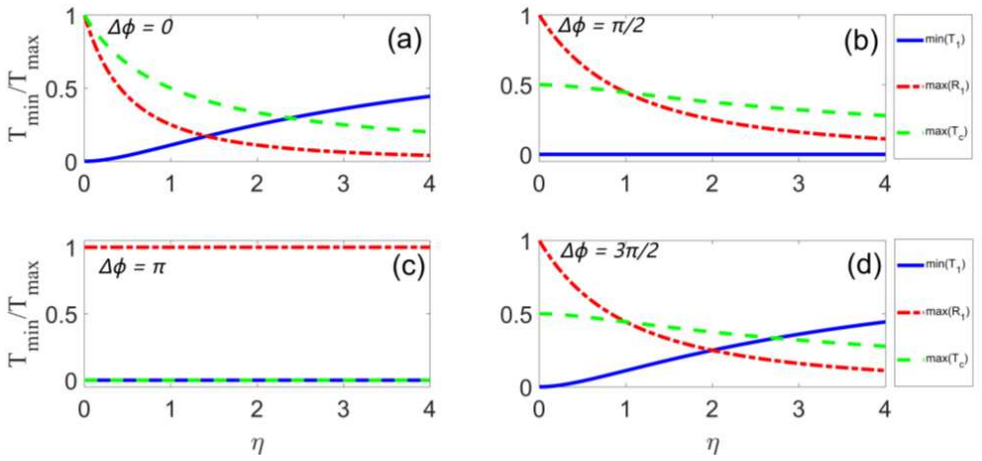

Figure 7. The effect of phase difference on the extreme values of transmission rate T_1, reflection rate R_1, and conversion efficiency T_c with different decay rates η. (**a**) The phase difference is set to be $\Delta\phi = 0$, (**b**) $\Delta\phi = \pi/2$, (**c**) $\Delta\phi = \pi$, and (**d**) $\Delta\phi = 3\pi/2$. Other parameters are $\phi_1 = 0$, $\gamma/\Gamma_1 = 0$, $\theta = 0$.

When $\Delta\phi$ continues to increase to π [see Figure 7c], the minimum of the transmission rate T_1 is always 0. The maximum value of the reflection rate R_1 is always 1. And the maximum value of the conversion efficiency T_c is always 0, i.e., $(T_c)_{\max} \equiv 0$. They do not change with a change in η, and the system shows the total reflection phenomenon, which is independent of the value of η. In Figure 7d, $(T_1)_{\min}$ is monotonically increasing when $\phi_1 = 0$ and $\Delta\phi = 3\pi/2$. There is a minimum value $(T_1)_{\min}$ occurring at $\eta = 0$. $(R_1)_{\max}$ and $(T_c)_{\max}$ are monotone decreasing curves, and the curves reach their maximum value at $\eta = 0$, which is 1.

We plot the scattering probability with detuning Δ and dissipation rate γ for phase $\phi_1 = 0$ and decay rate $\eta = 1$. In Figure 8a, we find that there is a minimum value of transmission rate, which occurs at $\gamma = 0$ and $\Delta = 0$. In addition, for the fixed value of γ, the transmission rate T_1 increases with an increase in the value of $|\Delta/\Gamma_1|$. In Figure 8b, the maximum of the reflection rate occurs at $\Delta = 0$ and $\gamma = 0$. Different from the transmission rate T_1, the reflection rate R_1 decreases with an increase in $|\Delta/\Gamma_1|$ when γ is fixed. In Figure 8c, we find that the optimal frequency conversion ($T_c = 0.5$) occurs at $\Delta = 0$ and $\gamma = 0$. In addition, with an increase in $|\Delta/\Gamma_1|$, the conversion efficiency T_c decreases gradually.

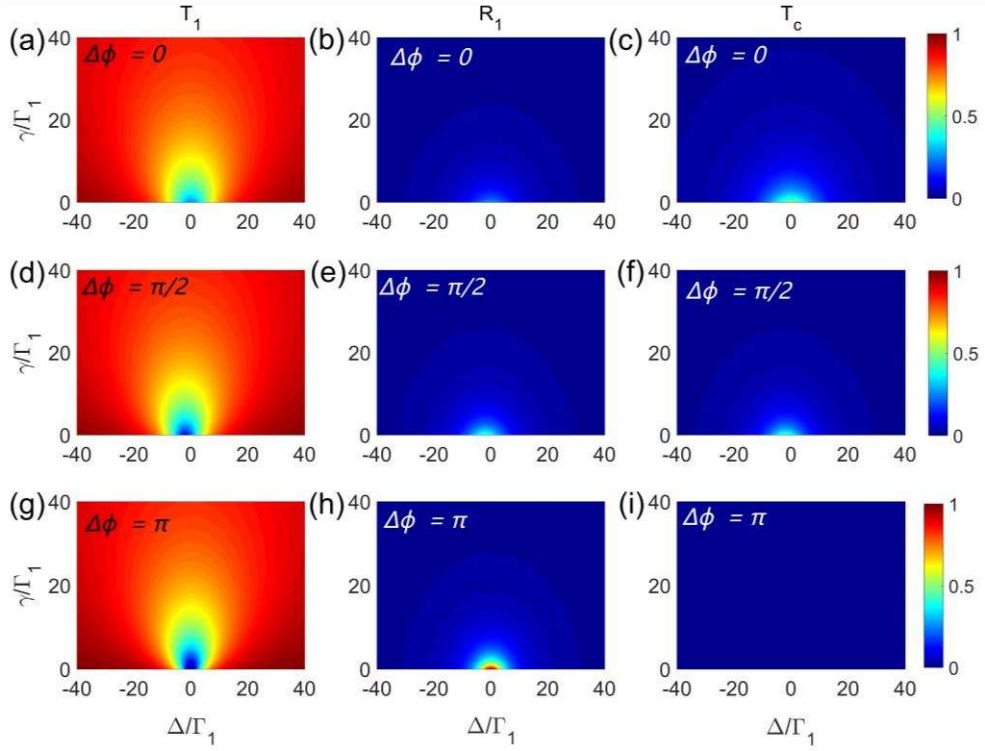

Figure 8. The effect of phase difference on the transmission rate T_1, reflection rate R_1, and conversion efficiency T_c with different detuning Δ/Γ_1 and dissipation rate γ. (**a**,**d**,**g**) The transmission rate T_1, (**b**,**e**,**h**) the reflection rate R_1, (**c**,**f**,**i**) the conversion efficiency T_c. We set the phase difference $\Delta\phi = 0$ in (**a**–**c**), $\Delta\phi = \pi/2$ in (**d**–**f**), and $\Delta\phi = \pi$ in (**g**–**i**). Other parameters are $\phi_1 = 0$, $\eta = 1$, $\theta = 0$.

When the phase difference $\Delta\phi$ increases to $\pi/2$, the minimum of the transmission rate occurs at $\Delta = -2\Gamma_1$ and $\gamma = 0$ [see Figure 8d]. Compared with Figure 8a, we find that the minimum of transmission rate decreases with an increase in phase difference. However, when γ is the fixed value, the transmission rate T_1 still increases with an increase in $|\Delta/\Gamma_1|$. Correspondingly, the maximum reflection rate increases with an increase in phase difference, and the maximum occurs at $\Delta = -2\Gamma_1$ and $\gamma = 0$ [see Figure 8e]. At this time, the system does not have an optimal frequency conversion, i.e., $T_c < 0.5$ [see Figure 8f].

When $\Delta\phi = \pi$, we find that the transmission rate T_1 obtains a minimum value of 0 at $\Delta = 0$ and $\gamma = 0$ [see Figure 8g]. The reflection rate R_1 obtains a maximum value of 1 at $\Delta = 0$ and $\gamma = 0$ [see Figure 8h]. And the conversion efficiency T_c is independent of γ and Δ, and its value is always 0 [see Figure 8i]. This phenomenon indicates that the photons are completely reflected in the system.

In order to more intuitively observe the transmission rate T_1, reflection rate R_1, and conversion efficiency T_c with respect to detuning Δ and dissipation rate γ, we take γ as $0, 10, 20, 30$ and draw Figure 9.

In Figure 9a, we find that the minimum transmission rate for phase difference $\Delta\phi = 0$ occurs at $\Delta = 0$ and $\gamma = 0$, which is 0.25. The minimum transmission rate increases with an increase in dissipation. Figure 9b,c show the reflection rate and conversion efficiency with detuning Δ at phase difference $\Delta\phi = 0$, respectively. In Figure 9b, the maximum reflection rate occurs at $\Delta = 0$ and $\gamma = 0$, which is 0.25. Unlike the transmission rate, the maximum reflection rate decreases with an increase in dissipation. In Figure 9c, we find that the system has an optimal frequency transition, and the optimal frequency transition occurs at $\Delta = 0$ and $\gamma = 0$ (solid blue line).

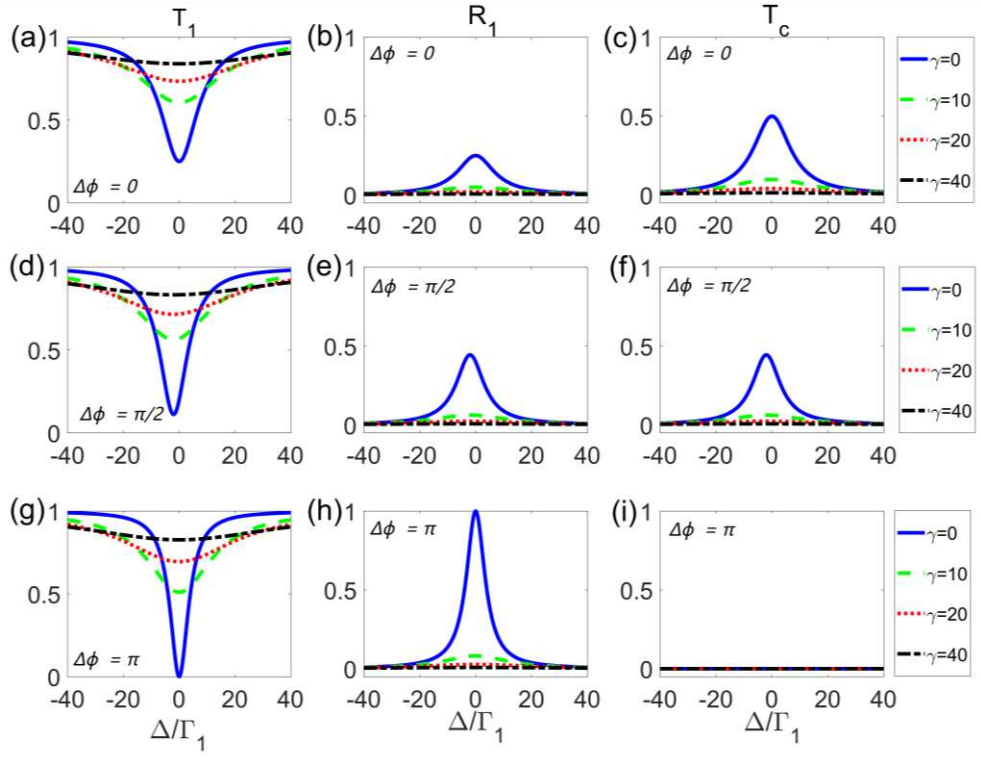

Figure 9. The change process of transmission rate T_1, reflection rate R_1, and conversion efficiency T_c with different detuning Δ/Γ_1 at different phase differences. (**a**,**d**,**g**) The transmission rate T_1, (**b**,**e**,**h**) the reflection rate R_1, (**c**,**f**,**i**) the conversion efficiency T_c. We set the phase difference $\Delta\phi = 0$ in (**a**–**c**), $\Delta\phi = \pi/2$ in (**d**–**f**), and $\Delta\phi = \pi$ in (**g**–**i**). Other parameters are $\phi_1 = 0$, $\eta = 1$, $\theta = 0$.

Figure 9d–f show the scattering rate with detuning Δ at phase difference $\Delta\phi = \pi/2$. At this time, the minimum of the transmission rate occurs at $\Delta = -2\Gamma_1$ and $\gamma = 0$, and its value is 0.1111 [see the blue solid line in Figure 9d]. In Figure 9e, we find that the maximum of the reflection rate also occurs at $\Delta = -2\Gamma_1$ and $\gamma = 0$, which is 0.4444. These indicate that there is no total reflection in the system when $\Delta\phi = \pi/2$. And unlike the case of $\Delta\phi = 0$, there is no optimal frequency conversion, i.e., $T_c < 0.5$ [see Figure 9f].

Figure 9g–i show the scattering rate with detuning Δ at phase difference $\Delta\phi = \pi$. At this time, the minimum of the transmission rate appears at $\Delta = 0$ and $\gamma = 0$, and its value is 0 [see the blue solid line in Figure 9g]. In Figure 9h, we find that the maximum of the reflection rate also occurs at $\Delta = 0$ and $\gamma = 0$, which is 1. These show that the total reflection occurs when $\Delta\phi = \pi$, and the conditions for the total reflection are $\Delta = 0$ and $\gamma = 0$. At this time, there is no optimal frequency conversion in the system [see Figure 9f].

In fact, the optimal frequency conversion ($T_c = 0.5$) occurs at $\Delta = 0$ and $\gamma = 0$ when $\phi_1 = 2m\pi$ and $\Delta = 0$. This phenomenon shows that when there is no atomic dissipation in the system, the system can achieve the optimal transmission rate of photons, which is 0.25. With an increase in dissipation, the number of transmitted photons decreases. When $\phi_1 = (2m+1)\pi$ and $\Delta\phi = \pi$, if there is no dissipation, the incident photon can be completely reflected and the photon cannot pass through the system.

We further change the dissipation rate and study the extreme values of transmission rate T_1, reflection rate R_1, and conversion efficiency T_c as γ changes [see Figure 10]. In Figure 10a, we find that the minimum of the transmission rate T_1 is monotonically increasing when $\phi_1 = 0$ and $\Delta\phi = 0$. Its minimum value occurs at $\gamma = 0$, which is 0.25. The maximum of reflection rate R_1 is the monotone decline curve, and its maximum value occurs at $\gamma = 0$, which is 0.25. The maximum of conversion rate T_c is the monotone decline curve with the maximum value of 0.5 at $\gamma = 0$. At this time, the system has the optimal frequency conversion. When the phase difference $\Delta\phi$ increases to $\pi/2$ [see Figure 10b], the minimum transmission rate T_1 is a monotonically increasing curve. Its minimum value

occurs at $\gamma = 0$, which is 0.1111. The maximum of reflection rate R_1 is a monotonically declining curve, and its maximum value occurs at $\gamma = 0$, which is 0.4444. The maximum of conversion rate T_c is a monotonically declining curve, and its maximum value occurs at $\gamma = 0$, which is $0.4444 < 0.5$. There is no optimal frequency conversion in the system.

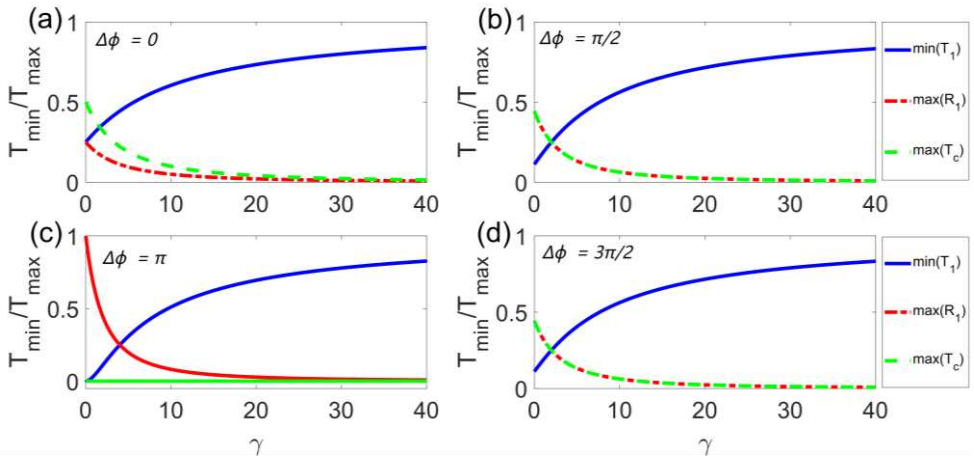

Figure 10. The effect of phase difference on the extreme values of transmission rate T_1, reflection rate R_1, and conversion efficiency T_c with different dissipation rates γ. (**a**) The phase difference is set to be $\Delta\phi = 0$, (**b**) $\Delta\phi = \pi/2$, (**c**) $\Delta\phi = \pi$, and (**d**) $\Delta\phi = 3\pi/2$. Other parameters are $\phi_1 = 0$, $\eta = 1$, $\theta = 0$.

When $\Delta\phi$ continues to increase to π [see Figure 10c], the minimum of the transmission rate T_1 appears at $\gamma = 0$, which is 0. The maximum of the reflection rate R_1 appears at $\gamma = 0$, and its value is 1. The maximum of the conversion rate T_c is always 0, i.e., $(T_c)_{\max} \equiv 0$. At this time, the system has the total reflection at $\gamma = 0$. Figure 10d shows the variation in the extreme values of the transmission rate T_1, reflection rate R_1, and conversion efficiency T_c with γ at $\Delta\phi = 3\pi/2$. In Figure 10d, we can see that the extreme values of the transmission rate T_1, reflection rate R_1, and conversion efficiency T_c are the same as those of the case of $\Delta\phi = \pi/2$.

According to Equations (7) and (10), the transmission rate T_1 and reflection rate R_1 are independent of the local coupling phase θ. Therefore, the effects of the locally coupled phase θ on the transmission rate and reflection rate are not discussed here. We analyze the changes in the conversion efficiency T_c with respect to detuning Δ and locally coupled phase θ [see Figure 11(a1–c1)]. In Figure 11(a1), there is a maximum transmission rate when $\Delta = 0$. The value of the maximum is 0. In Figure 11(b1), the reflection rate obtains a maximum of 0.4444 at $\Delta = -2\Gamma_1$ no matter how the value of θ changes. In Figure 11(c1), the conversion efficiency T_c is always 0 regardless of the value of θ.

Figure 11(a2–c2) shows the conversion efficiency T_c with respect to detuning Δ when $\Delta\phi$ is $0, \pi/2, \pi$, respectively. Obviously, the conversion efficiency T_c is independent of the local coupling phase no matter how $\Delta\phi$ varies [see Figure 11(a2–c2)]. When $\Delta\phi = 0$, conversion efficiency T_c obtains a maximum value of 0.5 at $\Delta = 0$ [see Figure 11(a2)]. When $\Delta\phi = \pi/2$, conversion efficiency T_c obtains a maximum value of 0.4444 at $\Delta = -2\Gamma_1$ [see Figure 11(b2)]. When $\Delta\phi = \pi$, the conversion efficiency is always 0, i.e., $T_c \equiv 0$ [see Figure 11(c2)].

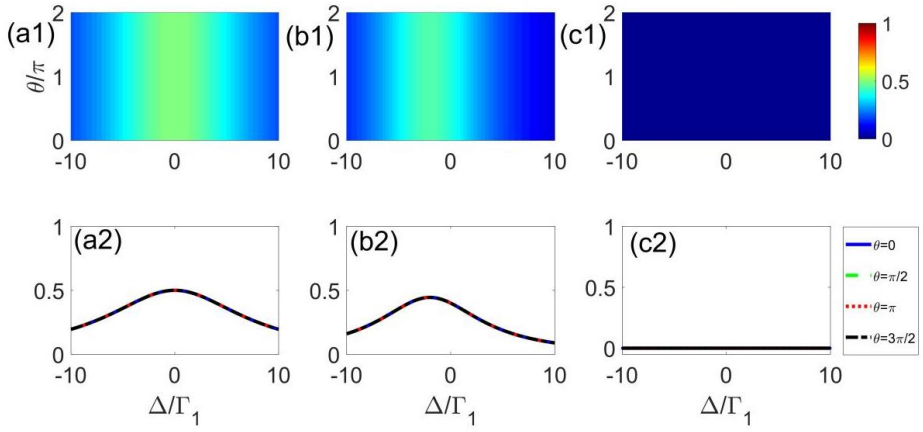

Figure 11. (**a1**–**c1**) The effect of phase difference on conversion efficiency T_c with different detuning Δ/Γ_1 and local coupling phases θ. (**a2**–**c2**) The change process of conversion efficiency T_c with different detuning Δ/Γ_1 at different phase differences. We set the phase difference $\Delta\phi = 0$ in (**a1**,**a2**), $\Delta\phi = \pi/2$ in (**b1**,**b2**), $\Delta\phi = \pi$ in (**c1**,**c2**). Other parameters are $\phi_1 = 0$, $\eta = 1$, $\gamma/\Gamma_1 = 0$.

4. Discussion

Firstly, for the arbitrary changes in the parameters in our model simulation, such as θ_1/θ_2, g_1/g_2, and ϕ_1/ϕ_2, we provide the following explanation. On one hand, we believe that changes in phase and coupling strength are very common in physical models. On the other hand, in ref. [35], it is mentioned that with superconducting quantum devices, the local coupling phases θ_1 and θ_2 can be introduced with Josephson loops threaded by external fluxes, and the coupling points can be encoded with different local phases. Ref. [33] has also studied single-photon scattering characteristics by changing the local coupling phase. From this perspective, the local coupling phase can be changed. In addition, Ref. [34] showed that when a three-level giant atom is coupled with a one-dimensional waveguide, g_1 and g_2 are the coupling strengths of transitions $|g\rangle \leftrightarrow |e\rangle$ and $|f\rangle \leftrightarrow |e\rangle$ with the waveguide modes, respectively. We believe that the coupling strengths g_1 and g_2 can change with the transformation of $|g\rangle \leftrightarrow |e\rangle$ and $|f\rangle \leftrightarrow |e\rangle$ in real experiments. It is mentioned in ref. [18] that both ϕ_1 and $\Delta\phi$ can be tuned within $[0, 2\pi]$ readily by adjusting the external parameters such as the voltages and currents or the electric and magnetic fields.

Secondly, we compare our results with previous works. In ref. [33], Chen et al. coupled two-level giant atoms with one-dimensional waveguides, and they found that the dissipation rate and local coupling phase have some interesting effects on the transmission rate and reflection rate of QED systems in giant atomic waveguides. In addition, their study of the non-trivial single-photon scattering properties of giant atomic waveguide QED systems provided an excellent platform for achieving nonreciprocal and chiral quantum optics. In ref. [12], Kockum et al. coupled multiple two-level giant atoms to one-dimensional waveguides and further showed that setups with giant atoms can be implemented in superconducting circuits. They also found that when two braided giant atoms were coupled to a waveguide, there was a decoherence-free interaction between the atoms. In ref. [34], Du et al. coupled three-level giant atoms with one-dimensional waveguides to study single-photon scattering. However, they did not consider the effects of the dissipation rate and the local coupling phase of the relative scattering rate of the system. In contrast, the scattering characteristics of three-level giant atoms coupled with one-dimensional waveguides are studied in more detail in our work, and the limit phenomena of the system are observed more clearly by drawing extreme value images.

In addition, we would like to make an outlook on our work. Giant atoms are emerging as a new, interesting field of quantum optics. We learned that excitons are quasi-particles that can transmit energy through solid materials and exhibit both atomic and solid characteristics. The Rydberg atom, which can lift an electron to a very large orbit, is a kind of giant atom. In ref. [40], Hu et al. found a Rydberg moiré exciton, which is the counterpart

of the solid Rydberg atom. Rydberg moiré excitons have similar properties to Rydberg atoms and are more compatible with modern semiconductor technology. Thus, there is a certain similarity between giant atoms and excitons. We believe that someday, excitons may be an appropriate achievement of artificial giant atoms. The limit phenomena studied in our paper, such as the total reflection and frequency-independent perfect transmission (FIPT), have potential applications in single-photon quantum communication and quantum information processing [34]. And the giant atomic waveguide QED system may be able to be used in the following projects: superradiance, ultrastrong coupling, generating nonclassical light, Matryoshka atoms, and chiral quantum optics [2].

5. Conclusions

We have considered the coupling of a giant Λ-type atom to a waveguide at two separate points and investigated the scattering of single photons on this atom. A single input photon can be transmitted directly through the waveguide and can also be inelastically scattered when the frequency is switched. In the case of small atoms, ref. [32] has shown that the scattering behavior of photons is determined only by the ratio of the radiation decay rates induced by the two waveguides. The results of this work have shown that the phase factors also affect the elastic and inelastic scattering of single photons in the giant atom model, where the phase factors are related to the frequency of the two transitions and the separation between the two coupling points. The presence of these two coupling points will produce a series of phase-dependent interference effects. The interference effect affects the scattering behavior by changing the transition frequency and decay rate of the atom. We found that by adjusting the phase, the giant atoms can exhibit phenomena such as perfect transmission and total reflection, where, as long as $\phi_2 = \phi_1 - \Delta\phi = (2m+1)\pi$, total reflection can be observed. More interestingly, when $\phi_1 = (2m+1)\pi$, the system achieves frequency-independent perfect transmission (FIPT) no matter how the value of $\Delta\phi$ changes. And due to the conservation of photon number, the sum of the transmission rate, reflection rate, and conversion efficiency is always 1 (i.e., $T_1 + R_1 + T_c \equiv 1$). When $\phi_1 = 2m\pi$ and $\Delta\phi = 0$, the optimal frequency conversion ($T_c = 0.5$) occurs at the decay ratio $\eta = 1$. It is the same with small atoms. And when $\phi_1 = 2m\pi$ and $\Delta\phi = \pi/2$, the optimal frequency conversion ($T_c = 0.5$) occurs at $\Delta = -4\Gamma_1$ and $\eta = 2$. The phenomenon shows how giant atoms differ from small atoms. In addition, we found that as the dissipation rate of giant atoms increases, the transmission rate of a single photon increases and the reflection rate decreases. The results of this work have potential application value in single-photon quantum communication and quantum information processing.

Author Contributions: Conceptualization, L.L. and W.Z.; methodology, L.L. and C.L.; software, L.L.; validation, W.Z. and Q.C.; formal analysis, Y.X.; investigation, X.W.; resources, Y.X. and Z.C.; data curation, X.F.; writing—original draft preparation, L.L.; writing—review and editing, Y.Z. and H.Y.; visualization, Q.C. and S.M.; supervision, C.L.; project administration, L.L. All authors have read and agreed to the published version of the manuscript.

Funding: This work was supported by the National Natural Science Foundation of China (Grant Nos.12375014 and 11875149), the Youth Jing-gang Scholars Program of Jiangxi Province, China, and the Program of Qing-jiang Excellent Young Talents, Jiangxi University of Science and Technology.

Data Availability Statement: Data are contained within the article.

Conflicts of Interest: The authors declare no conflicts of interest.

Appendix A

The derivation of t_1 from Equation (6) to Equation (7) is as follows

$$t_1 = 1 + \frac{g_1 e^{i\theta_1} u_e}{i v_g e^{i\phi_1/2}} + \frac{g_1 e^{i\theta_1} u_e}{i v_g e^{-i\phi_1/2}}, \tag{A1}$$

$$u_e = \frac{2g_1 e^{-i\theta_1} cos(\phi_1/2)}{\Delta + i\gamma + 2i\Gamma_1\left(1 + e^{i\phi_1}\right) + 2i\Gamma_2\left(1 + e^{i\phi_2}\right)}, \tag{A2}$$

We substitute Equation (A2) into Equation (A1), and obtain the following equations

$$\begin{aligned}
t_1 &= 1 + \frac{g_1 e^{i\theta_1}}{iv_g}\left(\frac{1}{e^{i\phi_1/2}} + \frac{1}{e^{-i\phi_1/2}}\right)u_e \\
&= 1 + \frac{g_1 e^{i\theta_1}\cdot 2cos(\phi_1/2)}{iv_g}u_e \\
&= 1 + \frac{g_1 e^{i\theta_1}\cdot 2cos(\phi_1/2)}{iv_g}\left(\frac{2g_1 e^{-i\theta_1}cos(\phi_1/2)}{\Delta+i\gamma+2i\Gamma_1\left(1+e^{i\phi_1}\right)+2i\Gamma_2\left(1+e^{i\phi_2}\right)}\right) \\
&= 1 + \frac{i\cdot g_1 e^{i\theta_1}\cdot 2cos(\phi_1/2)}{i^2 v_g}\left(\frac{2g_1 e^{-i\theta_1}cos(\phi_1/2)}{\Delta+i\gamma+2i\Gamma_1\left(1+e^{i\phi_1}\right)+2i\Gamma_2\left(1+e^{i\phi_2}\right)}\right) \\
&= 1 + \frac{-4ig_1^2 cos^2(\phi_1/2)}{v_g\left(\Delta+i\gamma+2i\Gamma_1\left(1+e^{i\phi_1}\right)+2i\Gamma_2\left(1+e^{i\phi_2}\right)\right)},
\end{aligned}$$

Make $\Gamma_1 = g_1^2/v_g$, and it follows from $cos^2\left(\frac{\phi_1}{2}\right) = \frac{1+cos(\phi_1)}{2}$

$$\begin{aligned}
t_1 &= 1 + \frac{-2i\Gamma_1(1+cos(\phi_1))}{\Delta+i\gamma+2i\Gamma_1\left(1+e^{i\phi_1}\right)+2i\Gamma_2\left(1+e^{i\phi_2}\right)} \\
&= \frac{\Delta+i\gamma-2i\Gamma_1 cos(\phi_1)+2i\Gamma_1 e^{i\phi_1}+2i\Gamma_2\left(1+e^{i\phi_2}\right)}{\Delta+i\gamma+2i\Gamma_1\left(1+e^{i\phi_1}\right)+2i\Gamma_2\left(1+e^{i\phi_2}\right)} \\
&= \frac{\Delta+i\gamma-2i\Gamma_1 cos(\phi_1)+2i\Gamma_1[cos(\phi_1)+isin(\phi_1)]+2i\Gamma_2\left(1+e^{i\phi_2}\right)}{\Delta+i\gamma+2i\Gamma_1\left(1+e^{i\phi_1}\right)+2i\Gamma_2\left(1+e^{i\phi_2}\right)} \\
&= \frac{\Delta+i\gamma-2\Gamma_1 sin(\phi_1)+2i\Gamma_2\left(1+e^{i\phi_2}\right)}{\Delta+i\gamma+2i\Gamma_1\left(1+e^{i\phi_1}\right)+2i\Gamma_2\left(1+e^{i\phi_2}\right)}.
\end{aligned}$$

The derivation of r_1, t_2 and r_2 is analogous.

References

1. Gustafsson, M.V.; Aref, T.; Kockum, A.F.; Ekstr?m, M.K.; Johansson, G.; Delsing, P. Propagating phonons coupled to an artificial atom. *Science* **2014**, *346*, 207. [CrossRef]
2. Kockum, A.F. Quantum optics with giant atoms–the first five years. *Math. Ind.* **2021**, *33*, 125–146.
3. Kockum, A.F.; Delsing, P.; Johansson, G. Designing frequency-dependent relaxation rates and Lamb shifts for a giant artificial atom. *Phys. Rev. A* **2014**, *90*, 013837. [CrossRef]
4. Guo, L.; Grimsmo, A.L.; Kockum, A.F.; Pletyukhov, M.; Johansson, G. Giant acoustic atom: A single quantum system with a deterministic time delay. *Phys. Rev. A* **2017**, *95*, 053821. [CrossRef]
5. Andersson, G.; Suri, B.; Guo, L.; Aref, T.; Delsing, P. Nonexponential decay of a giant artificial atom. *Nat. Phys.* **2019**, *15*, 1123. [CrossRef]
6. Guo, L.; Kockum, A.F.; Marquardt, F.; Johansson, G. Oscillating bound states for a giant atom. *Phys. Rev. Res.* **2020**, *2*, 043014. [CrossRef]
7. Kannan, B.; Ruckriegel, M.; Campbell, D.; Kockum, A.F.; Braumüller, J.; Kim, D.; Kjaergaard, M.; Krantz, P.; Melville, A.; Niedzielski, B.M.; et al. Waveguide quantum electrodynamics with superconducting artificial giant atoms. *Nature* **2020**, *583*, 775. [CrossRef] [PubMed]
8. Vadiraj, A.M.; Ask, A.; McConkey, T.G.; Nsanzineza, I.C.; Sandbo Chang, W.; Kockum, A.F.; Wilson, C.M. Engineering the level structure of a giant artificial atom in waveguide quantum electrodynamics. *Phys. Rev. A* **2021**, *103*, 023710. [CrossRef]
9. Longhi, S. Photonic simulation of giant atom decay. *Opt. Lett.* **2020**, *45*, 3017–3020. [CrossRef] [PubMed]
10. González-Tudela, A.; Sánchez Mu?oz, C.; Cirac, J.I. Engineering and Harnessing Giant Atoms in High-Dimensional Baths: A Proposal for Implementation with Cold Atoms. *Phys. Rev. Lett.* **2019**, *122*, 203603. [CrossRef] [PubMed]
11. Cai, Q.Y.; Jia, W.Z. Coherent single-photon scattering spectra for a giant-atom waveguide-QED system beyond the dipole approximation. *Phys. Rev. A* **2021**, *104*, 033710. [CrossRef]
12. Kockum, A.F.; Johansson, G.; Nori, F. Decoherence-Free Interaction between Giant Atoms in Waveguide Quantum Electrodynamics. *Phys. Rev. Lett.* **2018**, *120*, 140404. [CrossRef] [PubMed]
13. Soro, A.; Kockum, A.F. Chiral quantum optics with giant atoms. *arXiv* **2022**, arXiv:2106.11946v1. [CrossRef]
14. Wang, X.; Liu, T.; Kockum, A.F.; Li, H.-R.; Nori, F. Tunable Chiral Bound States with Giant Atoms. *Phys. Rev. Lett.* **2021**, *126*, 043602. [CrossRef] [PubMed]
15. Cheng, W.-J.; Wang, Z.-H.; Liu, Y.-X. Boundary effect and dressed states of a giant atom in a topological waveguide. *arXiv* **2021**, arXiv:2103.04542.
16. Roy, D.; Wilson, C.M.; Firstenberg, O. Strongly interacting photons in one-dimensional continuum. *Rev. Mod. Phys.* **2017**, *89*, 021001. [CrossRef]

17. Liao, Z.; Zeng, X.; Nha, H.; Zubairy, M.S. Photon transport in a one-dimensional nanophotonic waveguide QED system. *Phys. Scr.* **2016**, *91*, 063004. [CrossRef]
18. Gu, X.; Kockum, A.F.; Miranowica, A.; Liu, Y.-X.; Nori, F. Microwave photonics with superconducting quantum circuits. *Phys. Rep.* **2017**, *718–719*, 1–102.
19. Bello, M.; Platero, G.; Cirac, J.I.; González-Tudela, A. Unconventional quantum optics in topological waveguide QED. *Sci. Adv.* **2019**, *5*, eaaw0297. [CrossRef]
20. Fayard, N.; Henriet, L.; Asenjo-Garcia, A.; Chang, D.E. Many-body localization in waveguide quantum electrodynamics. *Phys. Rev. Res.* **2021**, *3*, 033233. [CrossRef]
21. Astafiev, O.; Zagoskin, A.M.; Abdumalikov, A.A.; Yu, A.P.; Yamamoto, T.; Inomata, K.; Nakamura, Y.; Tsai, J.S. Resonance fluorescence of a single artificial atom. *Science* **2010**, *327*, 840–843. [CrossRef]
22. Hoi, I.-C.; Wilson, C.M.; Johansson, G.; Palomaki, T.; Peropadre, B.; Delsing, P. Demonstration of a single-photon router in the microwave regime. *Phys. Rev. Lett.* **2011**, *107*, 073601. [CrossRef]
23. Jia, W.Z.; Wang, Z.D. Single-photon transport in a one-dimensional waveguide coupling to a hybrid atom-optomechanical system. *Phys. Rev. A* **2013**, *88*, 063821. [CrossRef]
24. Laakso, M.; Pletyukhov, M. Scattering of two photons from two distant qubits: Exact solution. *Phys. Rev. Lett.* **2014**, *113*, 183601. [CrossRef]
25. Roy, D. Two-photon scattering by a driven three-level emitter in a one-dimensional waveguide and electromagnetically induced transparency. *Phys. Rev. Lett.* **2011**, *106*, 053601. [CrossRef]
26. Zhou, L.; Gong, Z.R.; Liu, Y.X.; Sun, C.P.; Nori, F. Controllable scattering of a single photon inside a one-dimensional resonator waveguide. *Phys. Rev. Lett.* **2008**, *101*, 100501. [CrossRef]
27. Lund-Hansen, T.; Stobbe, S.; Julsgaard, B.; Thyrrestrup, H.; Sünner, T.; Kamp, M.; Forchel, A.; Lodahl, P. Experimental Realization of Highly Efficient Broad-band Coupling of Single Quantum Dots to a Photonic Crystal Waveguide. *Phys. Rev. Lett.* **2008**, *101*, 113903. [CrossRef]
28. Arcari, M.; S?llner, I.; Javadi, A.; Lindskov Hansen, S.; Mahmoodian, S.; Liu, J.; Thyrrestrup, H.; Lee, E.H.; Song, J.D.; Stobbe, S.; et al. Near-unity coupling efficiency of a quantum emitter to a photonic crystal waveguide. *Phys. Rev. Lett.* **2014**, *113*, 093603. [CrossRef] [PubMed]
29. Hoi, I.-C.; Kockum, A.F.; Tornberg, L.; Pourkabirian, A.; Johansson, G.; Delsing, P.; Wilson, C.M. Probing the quantum vacuum with an artificial atom in front of a mirror. *Nat. Phys.* **2015**, *11*, 1045. [CrossRef]
30. Wen, P.Y.; Kockum, A.F.; Ian, H.; Chen, J.C.; Nori, F.; Hoi, I.-C. Reflective amplification without population inversion from a strongly driven superconducting qubit. *Phys. Rev. Lett.* **2018**, *120*, 063603. [CrossRef] [PubMed]
31. Vetsch, E.; Reitz, D.; Sagué, G.; Schmidt, R.; Dawkins, S.T.; Rauschenbeutel, A. Optical Interface Created by Laser-Cooled Atoms Trapped in the Evanescent Field Surrounding an Optical Nanofiber. *Phys. Rev. Lett.* **2010**, *104*, 203603. [CrossRef]
32. Corzo, N.V.; Gouraud, B.; Chandra, A.; Goban, A.; Sheremet, A.S.; Kupriyanov, D.V.; Laurat, J. Large Bragg Reflection from One-Dimensional Chains of Trapped Atoms Near a Nanoscale Waveguide. *Phys. Rev. Lett.* **2016**, *117*, 133603. [CrossRef]
33. Chen, Y.-T.; Du, L.; Guo, L.Z.; Wang, Z.H.; Zhang, Y.; Li, Y.; Wu, J.-H. Nonreciprocal and chiral single-photon scattering for giant atoms. *Physics* **2022**, *5*, 215. [CrossRef]
34. Du, L.; Li, Y. Single-photon frequency conversion via a giant Λ-type atom. *Phys. Rev. A* **2021**, *104*, 023712. [CrossRef]
35. Wang, X.; Li, H.-R. Chiral Quantum Network with Giant Atoms. *arXiv* **2021**, arXiv:2106.13187. [CrossRef]
36. Shen, J.-T.; Fan, S. Theory of single-photon transport in a single-mode waveguide. I. Coupling to a cavity containing a two-level atom. *Phys. Rev. A* **2009**, *79*, 023837.
37. Bradford, M.; Shen, J.-T. Single-photon frequency conversion by exploiting quantum interference. *Phys. Rev. A* **2012**, *85*, 043814. [CrossRef]
38. Zhao, W.; Zhang, Y.; Wang, Z. Phase-modulated electromagnetically induced transparency in a giant-atom system within waveguide QED. *arXiv* **2021**, arXiv:2102.03697.
39. Bradford, M.; Obi, K.C.; Shen, J.-T. Efficient Single Photon Frequency Conversion Using a Sagnac Interferometer. *Phys. Rev. Lett.* **2012**, *108*, 103902. [CrossRef] [PubMed]
40. Hu, Q.Y.; Zhan, Z.; Cui, H.Y.; Zhang, Y.L.; Jin, F.; Zhao, X.; Zhang, M.J.; Wang, Z.C.; Zhang, Q.M.; Watanabe, K.; et al. Observation of Rydberg moiré excitons. *Science* **2023**, *380*, 1367–1372. [CrossRef] [PubMed]